Journal of Engineering and Applied Sciences 14 (Special Issue 9): 10622-10631, 2019
ISSN: 1816-949X
© Medwell Journals, 2019

Efficiency Optimization of Biological Photovoltaic Cells using Nano-Powered Electronic Circuits Technology

Alaa H. Mohammed
Department of Electrical and Electronic Engineering,
University Tun Hussein Onn Malaysia,
86400 Parit Raja, Johor, Malaysia

Abstract: This study present a new method for optimizing the power conversion efficiency of the Biological Photovoltaic cells (BPVs). In this method, the electronic circuits that operate within ultra low power range is used rather than propose new strategies for facilitating the electrons transfer to the anode inside the cell through design new electrodes coupled with the use of different species of photoautotrophic organisms. The proposed method includes building a Nano-Powered Transconductance Amplifier (NPTA) using the Electrically Programmable Analog Devices (EPAD). The NPTA is designed with a special topology, through which the output voltage is almost equal to the open-circuit voltage of the BPV cell and the output current is boosted by the large trans conductance of the NPTA. The new approach exhibits a large increase in the power conversion of the BPVs which can be utilized to power the electronic devices.

Key words: Design, organisms, NPTA, facilitating, electrodes, voltage

INTRODUCTION

Comparing to the Silicon-based Photovoltaic cells (SPVs), the design ofthe BPVs that based on the photosynthetic reaction is attracting substantial interest as a means for conversion of solar light energy into electrical power. This interest is due to the ease of design, low manufacturing cost and energy generation potential during the night as a result of being the electrons are stored inside the photoautotrophic organisms during daylight hours. The BPVs are characterized by a short-circuit current density with a low rate of the micro amps and open-circuit voltage with average value of 0.25 V (Kazemzadeh *et al*., 2017), making them less efficient in converting solar energy into electrical energy. Therefore, these cells suffer from a scant efficiency in the electrical power conversion comparing to the SPVs. Hence, the objective of this work is to produce commercial devices with low manufacturing cost and excellent energy conversion efficiency.

BPV systems are defined by the type of the biological materials that they employ such as aquatic plants, green algae and cyanobacteria and the mechanism of electrons transfer from the biological material to the anode. In principle, the process of the electrons generation is common to all of the BPV systems where the electrons are produced by the photoautotrophic organisms through light-driven oxidation of water. Based on the BPV system that utilize sub-cellular components or whole cell, the BPVs are divided into two sub-categories, sub-cellular BPVs and cellular BPVs (Bombelli *et al*., 2011).

Sub-cellular BPVs are those that use the Photosystem II (PSII) which is a biochemical mechanism through which the photoautotrophic organisms absorb light energy for photosynthesis (Badura *et al*., 2011). In this type of BPVs, some studies have utilized the thermophilic cyanobacterium in the light harvesting and energy generation as it is quite stable in its purified form (Kato *et al*., 2012). Using the technique of inserting a nanoelectrode into the chloroplast of the living cell, photosynthetic electrons (1.2 pA at 6 A m^{-2}) were directly extracted (mediator-free) from the living algal cell (Ryu *et al*., 2010), although, scale-up this technique would be difficult. Thylakoid membrane was used for photocurrent generation via. Indirect Extracellular Electron Transfer (IEET) where the composite resulting from thylakoid-carbon nanotube exhibited high photo-electrochemical activity under illumination (Calkins *et al*., 2013). However, the practical applications of the sub-cellular BPVs are restricted by the stability of the light harvesting components (Raven, 2011; Bombelli *et al*., 2011).

In the cellular BPVs, the oxygenic photosynthetic organisms are used to produce electrons through the photolysis of water and supply them to the anode without the aid of heterotrophic species. Notably, the photosynthetic organisms in the cellular BPVs can generate electronic current in the dark through the aerobic breakdown of the internal carbon reserves accumulated during the light (McCormick *et al*., 2011, 2015). Mostly, the use of the prokaryotic cyanobacteria (blue-green algae) has been preferred in the cellular BPVs over the eukaryotes due to its simple physiology where the

electron transfer across the membrane requires fewer steps (Schultze *et al*., 2009). Some studies utilized various species of the cyanobacteria including filamentous strains and unicellular strains to generate light-dependent current (Tsujimura *et al.*, 2001). Through utilizing lipid-soluble artificial electron mediators to extract the electrons from the photoautotrophic organisms, power outputs higher than a few mW have been achieved (Yagishita *et al*., 1997) but their addition can cause a significant reduction the organisms viability over time (Martens and Hall, 1994). Some researchers achieved a significant positive light response through coating the anodes of the photosynthetic microbial fuel cell with electrically conductive polymers (Zou *et al*., 2009). Other researchers achieved a maximum power output of 6 mW m^{-2} where they exhibited that a positive light response could be preserve for several weeks (Pisciotta *et al.*, 2010). Micro fluidic-based BPV showed the highest recorded power densities of 100 m W m^{-2} in the light and 80 mW m^{-2} in the dark (Bombelli *et al*., 2015). However, on basis of the data reported for all species of the filamentous cyanobacteria (phormidium), the current produced by the photoautotrophic organisms in BPVs that use H_2O as a substrate for electrons generation was calculated to be <0.5% of the total number of the electrons generated by water oxidation (Ochiai *et al*., 1983). This means that despite of the improvements made on the BPVs, these cells still suffer from scant efficiency in the electrical power conversion.

MATERIALS AND METHODS

Research method: In this research, due to the low operating voltages, the electrically programmed MOSFETs that having a threshold voltage of zero volt with a precision tolerances are used in design the proposed NPTA for optimize the power conversion efficiency of the BPVs. Electrical programming technique was designed especially for the MOSFETs to largely reduce the power dissipation and current leakage, through enabling precision control of a specific parameters such as the gate threshold voltage. This technique involves trimming the MOSFET gate with a floating gate of Polysilicon embedded in the MOSFET gate oxide (Anonymous, 2005). The trimmed gate is electrically programmed by injecting a charge of electrons with a sufficient energy (hot electrons) to enter the oxide layer through the floating gate in order to create an electrically programmable analog device. Once the electrical programming is done, the required voltage and current levels are stored indefinitely in the device. This type of the MOSFET which can be electrically programmed through the trimmed gate is called theEPAD MOSFET.

The EPAD MOSFETs are characterized as ultra low-powered normally-on devices with large trans conductance, even at very low supply voltages. These devices can be electrically programmed in matched pairs or individually within a dual and quad packages to enable independent control of each device. The EPAD MOSFETs were designed and built on a single monolithic chip by the Advanced Linear Devices, Inc. manufacturer in dual and quad packages to enable design a multiple cascaded stages operate at a very low bias voltage. Thereby, by using these devices, it is possible to built an ultra low-powered electronic circuits that operate at very low supply voltage. Consequently, the zero-threshold EPAD MOSFETs packages used in this work are the dual package ALD212900 and the quad package ALD310700. The dual package ALD212900 is a matched pair of N-channel zero-threshold EPAD MOSFETs characterized by the following features and applications (Anonymous, 2017a, b):

Features:

- Zero threshold V_{TH} = 0.00V±0.01V
- Offset voltage match to 2 mV/10 mV max
- Sub-threshold voltage (nano-power) operation
- Minimum operating voltage of less than 100 mV
- Minimum operating current of less than 1nA
- Minimum operating power of less than 1nW
- DC current gain of larger than 10^8 at 25°C
- High transconductance and output conductance
- Low ON drain-to-source resistance, R_{DS} (ON) of 14Ω
- Output current of higher than 50 mA
- Matched and tracked temp-coefficient
- Tight lot-to-lot parametric control (structurally similar)
- Positive, zero and negative V_{TH} temp-coefficient
- Low input capacitance and leakage currents

Applications:

- Low overhead current mirrors and current sources
- Zero power normally-on circuits
- Energy harvesting circuits
- Very low voltage analog and digital circuits
- Zero power fail-safe circuits
- Backup battery circuits and power failure detector
- Extremely low level voltage-clamps
- Extremely low level zero-crossing detector
- Matched source followers and buffers
- Precision current mirrors and current sources
- Matched capacitive probes and sensor interfaces
- Charge detectors and charge integrators
- High gain differential amplifier input stage
- Matched peak-detectors and level-shifters
- Multiple channel sample-and-hold switches
- Precision current multipliers
- Discrete matched analog switches and multiplexers
- Nano power discrete voltage comparators

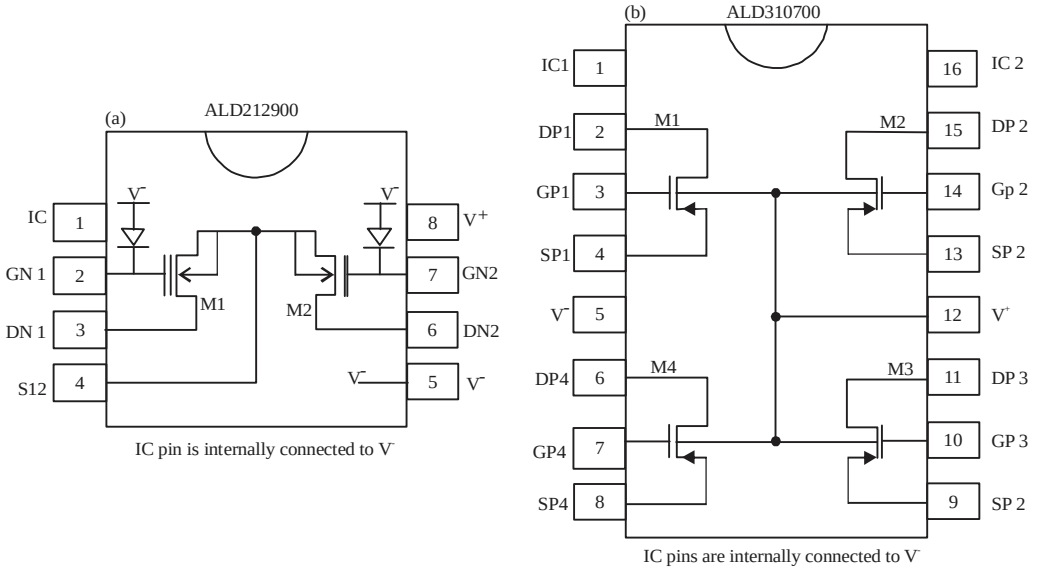

Fig. 1(a, b): Pin configuration of ALD212900 and ALD310700 packages

The quad package ALD310700 is a matched pair of P-channel zero-threshold EPAD MOSFETs characterized by the following features and applications (Anonymous, 201 a, b).

Features:

- Precision matched gate threshold voltages
- Precision offset voltages, 10 mV max
- Sub-threshold voltage operation
- Low min operating voltage of <0.2V
- Ultra low min operating current of <1nA
- Nano-power operation
- Wide dynamic operating current ranges
- Exponential operating current ranges
- Matched transconductance and output conductance
- Matched and tracked temperature characteristics
- Tight lot-to-lot parametric control (structurally similar)
- Positive, zero and negative V_{TH} temp-coefficient bias currents
- Low input capacitance
- Low input and output leakage currents

Applications:

- Precision current mirrors and current sources
- Low temp-coefficient (<= 50 ppm°C) current mirrors and sources
- Energy harvesting circuits
- Very low voltage analog and digital circuits
- Backup battery circuits and power failure detectors
- Precision low-level voltage clamps
- Low-level zero crossing detector

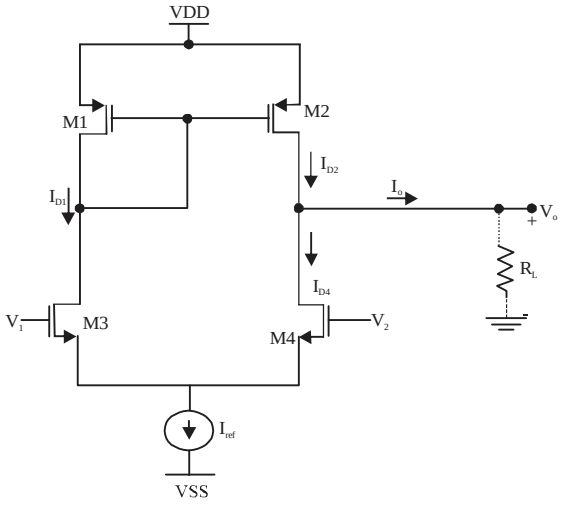

Fig. 2: The basic transconductance amplifier in the conventional MOSFETs structure

- Source followers and buffers
- Precision capacitive probes and sensor interfaces
- Precision charge detectors and charge integrators
- Discrete differential amplifier input stage
- Peak detectors and level shifters
- High-side switches and sample and hold switches
- Precision current multipliers
- Discrete analog switches and multiplexers
- Discrete voltage comparators

Figure 1 and 2 depicts the pin configuration of ALD212900 and ALD310700 packages.

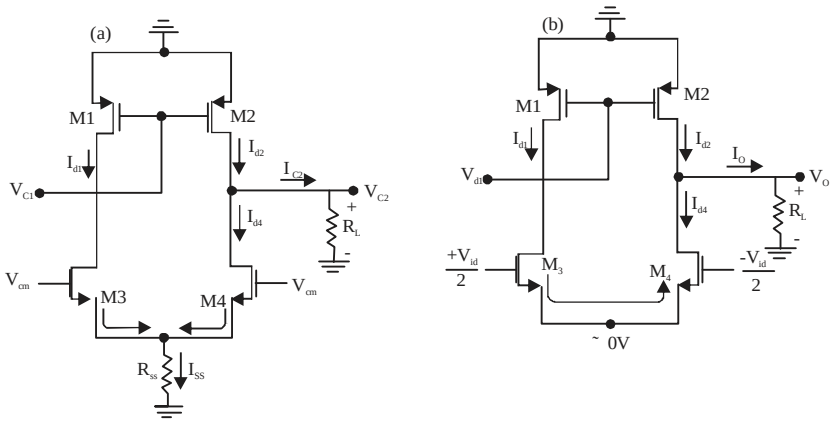

Fig. 3 (a, b): Equivalent circuits to (a) Common-mode and (b) Differential-mode

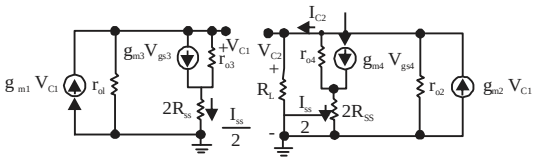

Fig. 4: Equivalent low-frequency circuit model to the comon-mode

NPTA design: In general, for analysing the trans conductance amplifier circuit, Fig. 2 shows the basic differential amplifier-based transconductance amplifier in the conventional MOSFETs structure where the conventional MOSFET equations also apply to the EPAD MOSFETs (Chao, 2015).

In the circuit of Fig. 1, practically it was observed that even if voltage V_1 and V_2 are equal, the output is not zero wh h reveals that the more realistic expression of V_1 and V_2 is:

$$V_1 = \frac{V_1+V_2}{2} + \frac{V_1-V_2}{2} = \frac{V_1+V_2}{2} + \frac{V_{id}}{2} = V_{cm} + \frac{V_{id}}{2} \quad (1)$$

$$V_2 = \frac{V_1+V_2}{2} - \frac{V_1-V_2}{2} = \frac{V_1+V_2}{2} - \frac{V_{id}}{2} = V_{cm} - \frac{V_{id}}{2} \quad (2)$$

where $V_{cm} = (V_1+V_2)^{-}2$ which is common to both V_1 and V_2 is called common-mode voltage. Hence, the practical transconductance amplifier operates in two modes, common-mode and differential-mode. To explain the operating in these two modes from Eq. 1 and 2, Fig. 3 shows the equivalent circuits to the common-mode and differential-mode.

where, V_{C1} and V_{C2} are the output voltages due to the common-mode R_{SS} which is of very large value is the shunt resistance of the open-circuit current I_{ref}, V_{d1} and V_o are the output voltages due to the differential-mode and $I_{SS} = I_{d1}+I_{d4}$.

In the practical differential amplifier, the common-mode Voltage V_{cm} which is a half sum of the input voltages is undesired signal because it causes a deviation from the ideality and the desired behaviour of the differential amplifier. This deviation is due to the amplification given to the V_{cm} that appears in the output. In the ideal differential amplifier, the common-mode voltage gain should be zero, so that, the output is not affected by the common-mode voltage. Based on modelling the MOSFET by its equivalent circuit to the low frequencies, Fig. 4 shows the equivalent low-frequency circuit model to the common-mode for determining the ideality condition in the performance from the circuit of Fig. 4:

$$V_{C1} = \left(g_{m1}V_{C1} - \frac{V_{C1}}{r_{o1}} - g_{m3}V_{gs3} \right) r_{o3} + R_{SS}I_{SS} \quad (3)$$

Or from the circuit of Fig. 3 a, since, $V_{gs3} = V_{cm}-R_{SS} I_{SS}$:

$$V_{C1} = \left[g_{m1}V_{C1} - \frac{V_{C1}}{r_{o1}} - g_{m3}\left(V_{cm} - R_{SS}I_{SS}\right) \right] r_{o3} + R_{SS}I_{SS} \quad (4)$$

Solving Eq. 4 for V_{C1} gives:

$$V_{C1} = \frac{R_{SS}I_{SS}\left(1+g_{m3}r_{o3}\right) - g_{m3}r_{o3}V_{cm}}{1 - r_{o3}\left(g_{m1} + \frac{1}{r_{o1}}\right)} \quad (5)$$

or since $(1/r_{o1}) << g_{m1}$:

$$V_{C1} \approx \frac{R_{SS}I_{SS}\left(1+g_{m3}r_{o3}\right) - g_{m3}r_{o3}V_{cm}}{1 - r_{o3}g_{m1}} \quad (6)$$

From the circuit of Fig. 4 where $V_{gs3} = V_{cm}-R_{SS} I_{SS}$

$$g_{m3}\left(V_{cm}-R_{SS}I_{SS}\right)+\frac{V_{C1}-R_{SS}I_{SS}}{r_{o3}}=\frac{I_{SS}}{2} \quad (7)$$

Since, R_{SS} is of very large value, then from the circuit of Fig. 4, could entirely drops on R_{SS} (R_{SS} I_{SS} $\approx V_{c1}$). Therefore, Eq. 7 can be approximated as:

$$g_{m3}\left(V_{cm}-R_{SS}I_{SS}\right)\approx\frac{I_{SS}}{2} \quad (8)$$

Solving Eq. 6 for I_{ss} gives:

$$I_{SS}\approx\frac{g_{m3}V_{cm}}{\frac{1}{2}+g_{m3}R_{ss}}\approx\frac{V_{cm}}{R_{ss}} \quad (9)$$

By substituting Eq. 9 in Eq. 6 and solving for V_{C1} yields:

$$V_{C1}\approx\frac{V_{cm}\left(1+g_{m3}r_{o3}\right)-g_{m3}r_{o3}V_{cm}}{1-r_{o3}g_{m1}}\approx\frac{-V_{cm}}{r_{o3}g_{m1}} \quad (10)$$

From the circuit of Fig. 4:

$$V_{C2}=I_{C2}R_L \quad (11)$$

$$I_{C2}=g_{m2}V_{C1}-\frac{V_{C2}}{r_{o2}}-g_{m4}V_{gs4}-\frac{V_{C2}-R_{SS}I_{SS}}{r_{o4}} \quad (12)$$

Substituting the value of I_{SS} from Eq. 9 and the value of V_{C1} from Eq. 10 in Eq. 12 where from the circuit of Fig. 3 a $V_{gs4}=V_{cm}-R_{SS}I_{SS}$ gives:

$$I_{C2}\approx\left(\frac{1}{r_{o4}}-\frac{g_{m2}}{g_{m1}r_{o3}}\right)V_{cm}-\frac{V_{C2}}{r_{o2}\|r_{o4}} \quad (13)$$

Thus, by substituting Eq. 13 in Eq. 11 and solving for yields:

$$V_{C2}\approx\frac{(1/r_{o4})-[g_{m2}/(g_{m1}r_{o3})]}{(1/R_L)+\left[1/\left(r_{o2}\|r_{o4}\right)\right]}V_{cm} \quad (14)$$

Hence, Eq. 14 states that the condition of suppressing V_{C2} which is the undesired output voltage resulting from the common-mode voltage is that both of M1, M2 and M3, M4 should be matching. This condition is achieved through utilizing the packages ALD212900 and ALD310700, since, they structurally contain of EPAD MOSFETs with a matched transconductance and output conductance. In case of that M1, M2 and M3, M4 are matching, differential amplifier-based transconductance amplifier will operate in the differential-mode only in order to achieve the ideality and the desired behaviour. Consequently, Fig. 5 shows the equivalent low-frequency circuit model to the differential-mode. From the circuit of Fig. 5:

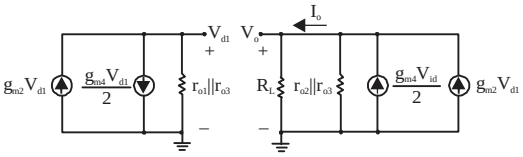

Fig. 5: Equivalent low-frequency circuit model to the differentia-mode

$$V_{d1}=[g_{m2}V_{d1}-(g_{m4}V_{id}/2)](r_{o1}\|r_{o3}) \quad (15)$$

Solving Eq. 15 for V_{d1} gives:

$$V_{d1}=\frac{-g_{m4}(r_{o1}\|r_{o3})}{2\left[1-g_{m2}\left(r_{o1}\|r_{o3}\right)\right]}V_{id}\approx\frac{g_{m4}}{2g_{m2}}V_{id} \quad (16)$$

$$V_o=I_oR_L \quad (17)$$

$$I_o=g_{m2}V_{d1}+(g_{m4}V_{id}/2)-\left[V_o/(r_{o2}r_{o3})\right] \quad (18)$$

Substituting the value of V_{d1} from Eq. 16 in Eq. 18 gives:

$$I_o\approx g_{m4}V_{id}-\left[V_o/(r_{o2}\|r_{o3})\right] \quad (19)$$

By substituting Eq. 19 in Eq. 17 and solving for yields:

$$V_o\approx\frac{g_{m4}R_L}{1+[R_L/(r_{o2}\|r_{o3})]}V_{id}\approx g_{m4}R_LV_{id} \quad (20)$$

Since, all devices should be in the saturation region (operating region), the saturation current (D_{SAT4}) of M4 by neglecting the channel length modulation parameter (λ) is given by:

$$I_{Dsat4}=\frac{\mu_e c_{ox}^{'}}{2}\left(W/L\right)_{M4}\left(V_{GS4}-V_{TH}\right)^2 \quad (21)$$

Thus, the transconductance, g_{m4} of M4 is:

$$g_{m4}=\frac{\partial I_{Dsat4}}{\partial V_{GS4}}=\mu_e c_{ox}^{'}\left(W/L\right)_{M4}\left(V_{GS4}-V_{TH}\right) \quad (22)$$

or from Eq. 21, since:

$$V_{GS4}-V_{TH}=\sqrt{\frac{2I_{Dsat4}}{\mu_e c_{ox}^{'}}\left(\frac{L}{W}\right)_{M4}} \quad (23)$$

$$g_{m4}=\sqrt{2\mu_e c_{ox}^{'}\left(W/L\right)_{M4}I_{Dsat4}} \quad (24)$$

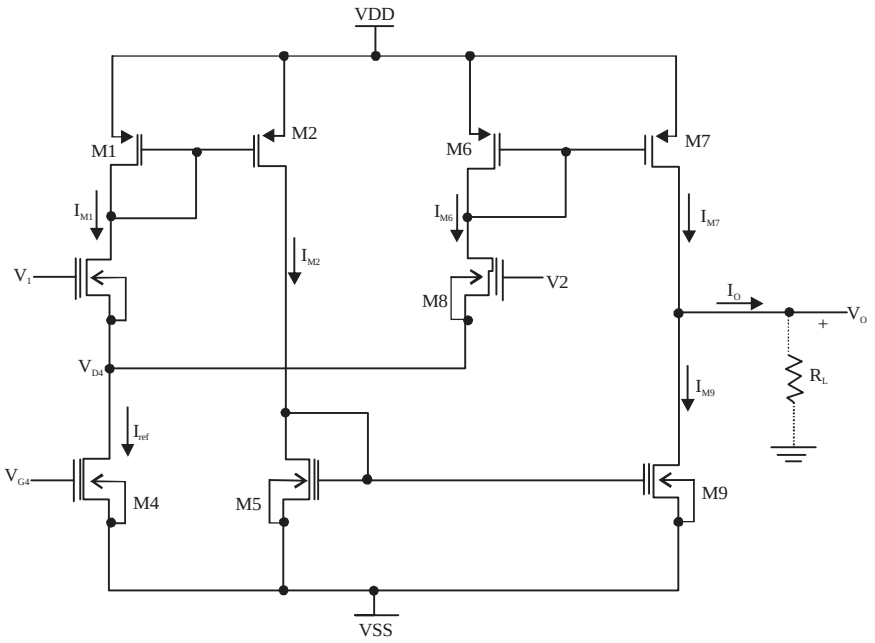

Fig. 6: The proposed topology of the NPTA

Hence, since, M3 and M4 are matching, then $I_{Dsat3} = I_{Dsat4}$. This means that $2I_{Dsat4} = I_{Dsat3}+I_{Dsat4} = I_{ref}$. Therefore, from Eq. 24, the transconductance g_{m4} of the transconductance amplifier is:

$$g_m = \sqrt{\mu_e c'_{ox} (W/L) I_{ref}} \quad (25)$$

where $(W/L) = (W/L)_{M4} = (W/L)_{M3}$. In general, the output Voltage, V_o of the transconductance amplifier is:

$$V_o = g_m R_L V_{id} \quad (26)$$

Hence, by substituting Eq. 25 in Eq. 26 yields:

$$V_o = \sqrt{\mu_e c'_{ox} \left(\frac{W}{L}\right) I_{ref}} \; R_L V_{id} \quad (27)$$

Thus, the output current, I_o of the transconductance amplifierin case of the differential-mode is:

$$I_o = \frac{V_o}{R_L} = \sqrt{\mu_e c'_{ox} \left(\frac{W}{L}\right) I_{ref}} \; V_{id} = g_m (V_1 - V_2) \quad (28)$$

From Eq. 25 and 28, it is observed that I_o of the transconductance amplifier that having matching MOSFETs can be boosted byboosting the I_{ref} and through using MOSSFETs having large transconductance such as the EPAD MOSFETs. Consequently, in this research, the packages ALD212900 and ALD310700 that contain of matching N and P-type EPAD MOSFETs with a largeare used in design the NPTA and the reference current I_{ref} is boosted through the proposed the topology which is shown in Fig. 6.

In this topology, the current is mirrored by the current I_{M1} mirror M1 and M2 on the drain of M2 (I_{M2}) and then, I_{M2} which is equal to I_{M1} is mirrored by the current mirror M5 and M9 on the drain of M9 (I_{M9}) to achieve that I_{M9} I_{M1} equals. The current I_{M6} which is the difference between I_{ref} and is mirrored by the current mirror M6 and M7 on the drain of M7 to achieve that I_{M7} equals I_{M6}. Thus:

$$I_o = I_{M7} - I_{M9} = I_{M6} - I_{M1} \quad (29)$$

Hence, since, M1, M6 and M3, M8 are matching(ALD310700 package and ALD212900 package, respectively), then, when no input voltages (V_1 and V_2) are applied I_{M6} is equal to I_{M1} or I_{M7} is equal to I_{M9}. Therefore, the undesired output current due to the bias requirements is zero even if the output is short circuited. Thus, there is no error ratio in the output and the load Voltage V_o is closely equal to the bias voltage VDD even with a very low load resistance. Through the proposed topology, the overall transconductance g_m of the NPTA can be increased through amplifying the reference current I_{ref} as long as from Eq. 25 g_m is directly proportional to I_{ref}. I_{ref} can beamplified through setting the drain-to-source

Voltage (V_{DS}) of the transistor M4 which is used as a current source to a large enough value that the drain to source current (I_{DS4}) of M4 which is the I_{ref} is saturated at the value set by the gate Voltage (V_{G4}). In this case, the drain-to-source voltage of M4 is much larger than the thermal Voltage (V_T) (V_{DS}>>.V_T) and the saturated I_{ref} can be modelled in the saturation region as:

$$I_{ref} = I_{DS4} \approx I_{D0}\, e^{\frac{V_{GS}-V_{TH}}{\eta V_T}} \quad (30)$$

Formulation of Eq. 30 in the saturation region, comes from the drain-to-source current (I_{DS}) relationship with the gate-to-source Voltage (V_{GS}) and drain-to-source voltage V_{DS} in the sub-threshold region (weak inversion) which is given by the exponential relationship (Arora, 1993):

$$I_{DS} = I_{D0}\, e^{\frac{V_{GS}-V_{TH}}{\eta V_T}}\left(1-e^{-\frac{V_{DS}}{V_T}}\right) \quad (31)$$

where:

$$I_{D0} = \frac{\mu_e V_T^2 W}{L}\sqrt{\frac{qN_A \in_{si}}{2\left(\frac{V_{GS}-V_{TH}}{\eta}-2V_p\right)}} \quad (32)$$

Where

μ_e : The electron mobility [cm^2 (V.s)]

V_T =kT/q : The thermal voltage where k = 1.38×10^{-23} J/°K is the Boltzmann's constant

T = The temperature in Kelvin and q = 1.6×10^{-19} Coulombs is the electron charge

W : The gate Width

L : The gate Length

N_A : The holes concentration

V_p : The drop voltage across the gate-oxide region and

$$\eta \equiv 1+\frac{1}{c'_{ox}}\sqrt{\frac{\grave{o}_{si}qN_A}{2(-2V_p)}} \quad (33)$$

where c'$_{ox}$ is the gate oxide capacitance per unit area and $\in_{si}$ is the silicon permittivity to the electric field. Thus, it is observed from Eq. 31 in case of that V_{DS}>>V_T the dependence of I_{DS} on the V_{DS} can be neglected but not completely because there is a residual sensitivity of theI_{DS} toV_{DS}. This case is similar to the saturation region for strong inversion. Therefore, on the condition that V_{DS}>>I_{DS} in the saturation region is given by Eq. 30. Hence, from the circuit of Fig. 6, since, the gate-to-source Voltage (V_{GS4}) of M4 is:

$$V_{GS4} = V_{G4} - VSS \quad (34)$$

then by substituting Eq. 34 in Eq. 30, yields:

$$I_{ref} = I_{D0}\, e^{\frac{(V_{G4}-VSS)-V_{TH}}{\eta V_T}} \quad (35)$$

or since, the MOSFETs used in this work are matching EPAD MOSFETs of zero threshold Voltage (V_{TH} = 0), the reference current in the saturation region can be approximately modelled as:

$$I_{ref} \approx I_{D0}\, e^{\frac{(V_{G4}-V_{SS}}{\eta V_T}} \quad (36)$$

Consequently, since all EPAD MOSFETs are in the saturation region (V_{DS}>>V_T), the transconductance g_m of the proposed NPTA can be derived as following:

$$I_{M1} \approx I_{D0}\, e^{\frac{V_1-V_{D4}}{\eta V_T}} = I_{D0}\, e^{-\alpha V_{D4}}\, e^{\alpha V_1} \quad (37)$$

$$I_{M6} \approx I_{D0}\, e^{\frac{V_2-V_{D4}}{\eta V_T}} = I_{D0}\, e^{e-\alpha V_{D4}}\, e^{\alpha V_2} \quad (38)$$

$$I_{ref} = I_{M1}+I_{M6} = I_{D0}\, e^{-\alpha V_{D4}}\left(e^{\alpha V_1}+e^{\alpha V_2}\right) \quad (39)$$

where, $\alpha = 1/(\eta V_T) = q/(\eta kT)$. Hence, from Eq. 39:

$$e^{-\alpha V_{D4}} = \frac{I_{ref}}{I_{D0}}\frac{1}{e^{\alpha V_1}+e^{\alpha V_2}} \quad (40)$$

Substituting Eq. 40 in Eq. 37 and 38, respectively gives:

$$I_{M1} \approx I_{ref}\frac{e^{\alpha V_1}}{e^{\alpha V_1}+e^{\alpha V_2}} \quad (41)$$

$$I_{M6} \approx I_{ref}\frac{e^{\alpha V_2}}{e^{\alpha V_1}+e^{\alpha V_2}} \quad (42)$$

Thus, since, $I_{M1} = I_{M9}$ and $I_{M6} = I_{M7}$

$$I_o = I_{M6}-I_{M1} = -I_{ref}\frac{e^{\alpha V_1}-e^{\alpha V_2}}{e^{\alpha V_1}+e^{\alpha V_2}} \quad (43)$$

Multiplying both the nominator and denominator of Eq. 43 by $e^{-\alpha(V1+V2)/2}$ gives:

$$I_o = I_{ref}\frac{e^{\alpha(V_1-V_2)/2}-e^{-\alpha(V_1-V_2)/2}}{e^{\alpha(V_1-V_2)/2}+e^{-\alpha(V_1-V_2)/2}} = -I_{ref}\tanh\left[\frac{\alpha(V_1-V_2)}{2}\right] \quad (44)$$

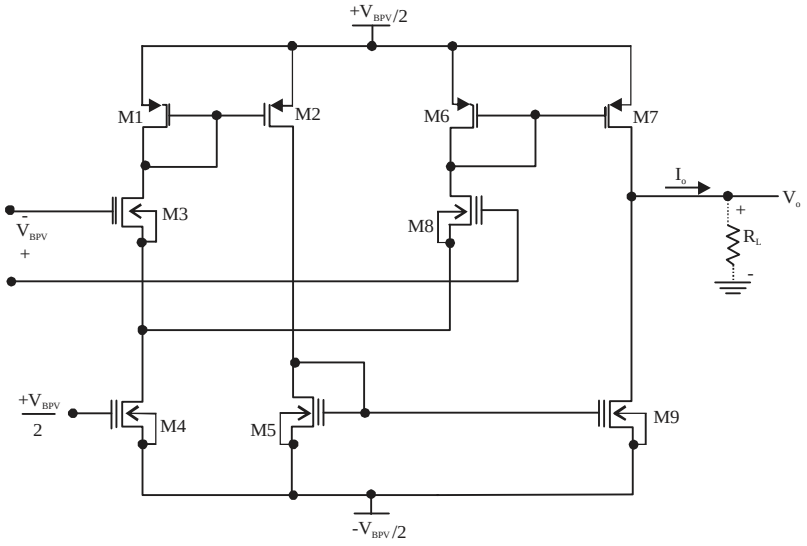

Fig. 7: The proposed NPTA using the open-circuit voltage of the BPV cell

Hence, the transconductance g_m of the proposed NPTA is the slop of the hyperbolic tan in Eq. 44 at the origin, i.e:

$$g_m = \left.\frac{\partial I_o}{\partial (V_1\text{-}V_2)}\right|_{V_1\text{-}V_2=0} = \frac{-\alpha I_{ref}}{2}\operatorname{sech}^2\left[\left.\frac{\alpha (V_1\text{-}V_2)}{2}\right]\right|_{V_1\text{-}V_2=0} \quad (45)$$

or since, $\operatorname{sech}^2 [\alpha(V_1\text{-}V_2)/2]|_{V1\text{-}V2 = 0} = 1$

$$g_m = \frac{-\alpha I_{ref}}{2} = \frac{I_{ref}}{2\eta kT/q} \quad (46)$$

Equation 46 states that the overall g_m of the NPTA can be increased by boosting the reference current I_{ref} through the gate Voltage, V_{G4} of the transistor M4. Thus, the output current of the proposed NPTA is:

$$I_o = g_m (V_1\text{-}V_2) = \frac{-I_{ref}}{2\eta kT/q}(V_1\text{-}V_2) \quad (47)$$

Hence, by utilizing the open-circuit Voltage (V_{BPV})of the BPV cell if $V_1 = -V_{BPV}/2$, $V_2 = +V_{BPV}/2$, VDD = $+V_{BPV}/2$, VSS = $-V_{BPV}/2$ and $V_{G4} = +V_{BPV}/2$ then from Eq. 47, the output current of the NPTA is expressed as:

$$I_o = \frac{I_{ref}}{2\eta kT/q} V_{BPV} \quad (48)$$

Equation 48 states that the output current of the proposed NPTA depends on both the overall transconductance g_m and the open-circuit voltage of the BPV cell. Accordingly, Fig. 7 shows the proposed NPTA using the open-circuit Voltage V_{BPV} of the BPV cell.

RESULTS AND DISCUSSION

The electricity/area produced to be easily measured, the BPV cell used in this work was constructed using the Acrylic sheets by two cylindrical chambersseparated by a Proton Exchange Membrane (PEM) of Nafion 117 the anodic chamber (diameter 10 cm and height 6 cm) and cathodic chamber (diameter 10 cm and height 2 cm). The anodic chamber was provided with one sealable opening which is necessary for performing the auxiliary operative activities while the cathodic chamber is open to the air to guarantee the presence of oxygen required for the cathodic reaction. The anode material chosen is Indium Tin Oxide (ITO) which is an effective material for electrons harvesting while the cathode material chosen is copper. In this cell, the living organism which is used as a harvesting material of the light is the cyanobacteria as it is capable of self-assembly and self-repair inside the cell.

The BPV cell performance was evaluated at 300°K, without using the proposed NPTA by means of polarization curve through varying the external Resistance (R_L) from 2 MΩ to 5 Ω where the voltages decrease from 150 to 10 mV while the current densities increase from 0-1.25 mA/m^2 as reported in Fig. 8.

To evaluate the performance of the BPV cell in the power conversion without using the NPTA, the power curve was reported as shown in Fig. 9 where basing on the maximum power transfer theorem, the cell internal resistance of 120 Ω was calculated.

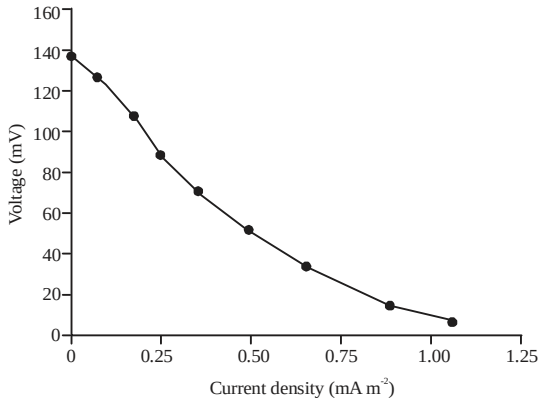

Fig. 8: The polarization curve of the BPV cell without using the proposed NPTA

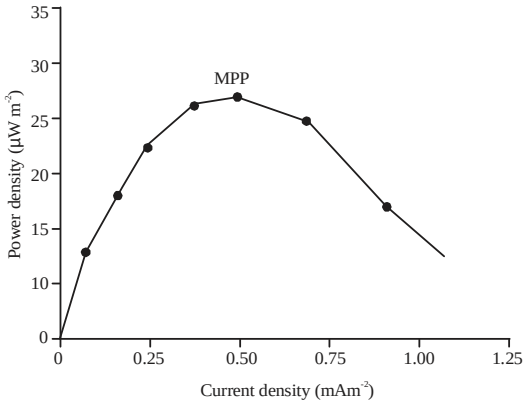

Fig. 9: The power curve of the BPV cell without using the proposed NPTA

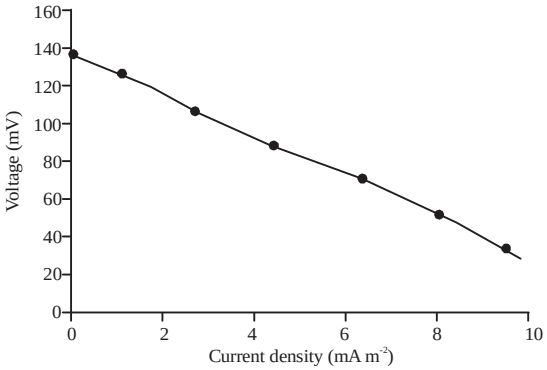

Fig. 10: The polarization curve of the BPV cell using the proposed NPTA

In comparison, the polarization curve and the power curve of the BPV cell using the proposed NPTA are reported as shown in Fig. 10 and 11, respectively through varying the external resistance from 2 MΩ to 5 Ω at 300°K.

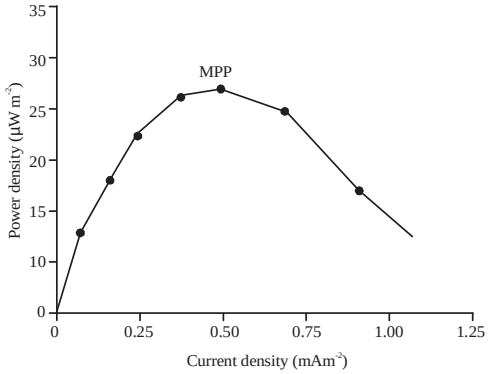

Fig. 11: The power curve of the BPV cell using the proposed NPTA

It is observed from Fig. 9 that without using the proposed NPTA, a Maximum Power Point (MPP) of 0.3 μW was recorded for the BPV cell under illumination, corresponding to a current density of 0.5 mA/m^2 and a voltage of 60 mV. While from Fig. 11 by using the proposed NPTA, the MPP recorded is 5.84 μW corresponding to a current density of 7.3 mAm^2 and a voltage of 80 mV.

CONCLUSION

In this study, a new approach to optimize electrical power conversion potential of the BPVs was proposed through utilizing the nano-powered electronic circuit rather than using different strategies for develop the cell design. The proposed method exhibited a large increase in the maximum power conversion (from 0.3-5.84 μW). Which means that an increase of 20 times in the output power has been achieved from the BPV cell by using the nano-powered electronic circuit technology. Thus an effective power can be obtained from the BPVs to power the electronic devices through using array of cells for increasing the output maximum power point.

ACKNOWLEDGEMENTS

The researchers would like to thank University Tun Hussein Onn Malaysia (UTHM) and Dr. Nafarizal and Dr. Izhal in particular for supporting this project.

REFERENCES

Anonymous, 2005. Chip trimming pushes Mosfet threshold to 0.2V. Electronics Weekly, UK. https://www.electronicsweekly.com/news/products/analog/chip-trimming-pushes-mosfet-threshold-to-0-2v-2005-09.

Anonymous, 2017a. Precision n-channel EPAD® mosfet array dual high drive zero threshold™ matched pair. Advanced Linear Devices Inc., Sunnyvale, California, USA. http://www.aldinc.com/pdf/ALD212900.pdf.

Anonymous, 2017b. Precision p-channel EPAD® mosfet array quad zero threshold™ matched pair. Advanced Linear Devices Inc., Sunnyvale, California, USA. http://www.aldinc.com/pdf/ALD310700.pdf.

Arora, N.D., 1993. MOSFET Models for VLSI Cizcuit Simulation: Theory and Practice. Springer, Wien, Austria, ISBN: 9783211823958, Pages: 605.

Badura, A., T. Kothe, W. Schuhmann and M. Rogner, 2011. Wiring photosynthetic enzymes to electrodes. Energy Environ. Sci., 4: 3263-3274.

Bombelli, P., R.W. Bradley, A.M. Scott, A.J. Philips and A.J. McCormick *et al.*, 2011. Quantitative analysis of the factors limiting solar power transduction by *Synechocystis sp*. PCC 6803 in biological photovoltaic devices. Energy Environ. Sci., 4: 4690-4698.

Bombelli, P., T. Muller, T.W. Herling, C.J. Howe and T.P. Knowles, 2015. A high power-density, mediator-free, microfluidic biophotovoltaic device for Cyanobacterial cells. Adv. Energy Mater., Vol. 5, No. 2. 10.1002/aenm.201401299

Calkins, J.O., Y. Umasankar, H. O'Neill and R.P. Ramasamy, 2013. High photo-electrochemical activity of thylakoid-carbon nanotube composites for photosynthetic energy conversion. Energy Environ. Sci., 6: 1891-1900.

Chao, R., 2005. Designing with ultra-low voltage MOSFET arrays. AspenCore Inc, Cambridge, Massachusetts, (USA). https://www.edn.com/design/automotive-design/4009586/Designing-with-ultra-low-voltage-MOSFET-arrays

Kato, M., T. Cardona, A.W. Rutherford and E. Reisner, 2012. Photoelectrochemical water oxidation with photosystem II integrated in a mesoporous indium-tin oxide electrode. J. Am. Chem. Soc., 134: 8332-8335.

Kazemzadeh, S., G. Riazi and R. Ajeian, 2017. Novel approach of biophotovoltaic solid state solar cells based on a multilayer of PS1 complexes as an active layer. ACS. Sustainable Chem. Eng., 5: 9836-9840.

Martens, N. and E.A. Hall, 1994. Diaminodurene as a mediator of a photocurrent using intact cells of Cyanobacteria. Photochem. Photobiol., 59: 91-98.

McCormick, A.J., P. Bombelli, A.M. Scott, A.J. Philips, A.G. Smith, A.C. Fisher and C.J. Howe, 2011. Photosynthetic biofilms in pure culture harness solar energy in a mediatorless bio-photovoltaic cell (BPV) system. Energy Environ. Sci., 4: 4699-4709.

McCormick, A.J., P. Bombelli, R.W. Bradley, R. Thorne, T. Wenzel and C.J. Howe, 2015. Biophotovoltaics: Oxygenic photosynthetic organisms in the world of bioelectrochemical systems. Energy Environ. Sci., 8: 1092-1109.

Ochiai, H., H. Shibata, Y. Sawa, M. Shoga and S. Ohta, 1983. Properties of semiconductor electrodes coated with living films of Cyanobacteria. Applied Biochem. Biotechnol., 8: 289-303.

Pisciotta, J.M., Y. Zou and I.V. Baskakov, 2010. Light-dependent electrogenic activity of Cyanobacteria. PLOS One, Vol. 5, No. 5. 10.1371/journal.pone.0010821

Raven, J.A., 2011. The cost of photoinhibition. Physiol. Plant., 142: 87-104.

Ryu, W., S.J. Bai, J.S. Park, Z. Huang, J. Moseley, T. Fabian and F.B. Prinz, 2010. Direct extraction of photosynthetic electrons from single algal cells by nanoprobing system. Nano Lett., 10: 1137-1143.

Schultze, M., B. Forberich, S. Rexroth, N.G. Dyczmons, M. Roegner and J. Appel, 2009. Localization of cytochrome b6f complexes implies an incomplete respiratory chain in cytoplasmic membranes of the Cyanobacterium *Synechocystis* sp. PCC 6803. Biochim. Biophys. Acta (BBA)-Bioenerg., 1787: 1479-1485.

Tsujimura, S., A. Wadano, K. Kano and T. Ikeda, 2001. Photosynthetic bioelectrochemical cell utilizing Cyanobacteria and water-generating oxidase. Enzyme Microb. Technol., 29: 225-231.

Yagishita, T., S. Sawayama, K.I. Tsukahara and T. Ogi, 1997. Behavior of glucose degradation in *Synechocystis* sp. M-203 in bioelectrochemical fuel cells. Bio Electrochem. Bioenerg., 43: 177-180.

Zou, Y., J. Pisciotta, R.B. Billmyre and I.V. Baskakov, 2009. Photosynthetic microbial fuel cells with positive light response. Biotechnol. Bioeng., 104: 939-946.